Robotica: (2020) volume 38, pp. 1227–1241. © Cambridge University Press 2019
doi:10.1017/S0263574719001371

A Human-Guided Vision-Based Measurement System for Multi-Station Robotic Motion Platform Based on V-Rep

Yabin Ding†*, Wei Guo†, Xianping Liu‡ and Zhenjun Luo†

†*Key Laboratory of Mechanism Theory and Equipment Design of Ministry of Education, Tianjin University, Tianjin, 300354, China.*
E-mails: ybding@tju.edu.cn, 1837825836@qq.com, zhenjunluo@tju.edu.cn
‡*School of Engineering, University of Warwick, Coventry, UK. E-mail: X.Liu@warwick.ac.uk*

(Accepted September 1, 2019. First published online: September 27, 2019)

SUMMARY
In the manufacturing process of sophisticated and individualized large components, classical solutions to build large machine tools cannot meet the demand. A hybrid robot, which is made up of a 3 degree-of-freedom (3-DOF) parallel manipulator and a 2-DOF serial manipulator, has been developed as a plug-and-play robotized module that can be rapidly located in multi-stations where machining operations can be performed *in situ*. However, processing towards high absolute accuracy has become a huge challenge due to the movement of robot platform. In this paper, a human-guided vision system is proposed and integrated in the robot system to improve the accuracy of the end-effector of a robot. A handheld manipulator is utilized as a tool for human–robot interaction in the large-scale unstructured circumstances without intelligence. With 6-DOF, humans are able to manipulate the robot (end-effector) so as to guide the camera to see target markers mounted on the machining datum. Simulation is operated on the virtual control platform V-Rep, showing a high robust and real-time performance on mapping human manipulation to the end-effector of robot. And then, a vision-based pose estimation method on a target marker is proposed to define the position and orientation of machining datum, and a compensation method is applied to reduce pose errors on the entire machining trajectory. The algorithms are tested on V-Rep, and the results show that the absolute pose error reduces greatly with the proposed methods, and the system is immune to the motion deviation of the robot platform.

KEYWORDS: Human-guided manipulator; Vision-based measurement system; Pose estimation; 5-DOF hybrid robot; V-Rep.

1. Introduction

Large-volume manufacturing industries, for example, aeronautics, astronautics, and shipping, are looking for cost-effective flexible solutions to meet the ever-increasing customer demands toward high speed and high quality.[1] Instead of the classical and most frequent solution to machining very large parts, which is to build very large machine tools with serial travels, a 5 degree-of-freedom (5-DOF) hybrid kinematic machine[2] (or a hybrid robot which is made up of a 3-DOF parallel manipulator and a 2-DOF serial manipulator) shows a huge potential to meet these requirements. They are adequate where bigger forces and accuracies are required, but still maintaining the necessary stiffness that articulated robots cannot offer. For example, they have been used in aerospace applications

* Corresponding author. E-mail: ybding@tju.edu.cn

when bigger stiffness and harder materials need to be machined. Some types of hybrid robots have been proposed over the last decade, such as Tricept,[3] Exechon,[2] and TriMule[4] (which was designed in our recent work). These hybrid robots can be built as a plug-and-play robotized module mounted on a long reference track (motion platform) so that it can be rapidly located in the multi-stations where machining needs to be performed *in situ*. However, motion platform brings great challenges to robot processing accuracy. Errors will be induced when the robot moves between the stations, and will be magnified in a certain degree on the position of robot effector, which directly affects the pose of machining trajectory.

Locating accuracy and efficiency are important performances of the above-mentioned hybrid robots when they are applied for machining in multi-stations. Current robots generally achieve a high repeatability. For example, the repeatability of a KUKA KR210 can reach ± 0.06 mm, whereas the absolute accuracy is only ± 3 mm. The absolute positioning accuracy cannot meet the high precision requirement of ± 0.5 mm in aircraft assembly.[5] Motivated by these requirements, in order to obtain the ultimate accuracy performance, the current trend in large-volume manufacturing is to integrate the measurement system[6] to the robot system, using a laser interferometer, absolute distance-measuring systems, and charge-coupled device (CCD) cameras.

The most commonly used measurement system based on laser interference is the laser tracker system (LTS), which consists of an interferometric distance-measuring device, angular sensors of the beam-guiding system, and a tracking system. Vincze put forward a real-time method of measuring position and orientation of end-effector of robots utilizing a laser tracker and a vision system.[7] Flynn used laser trackers with a self-positioning spherically mounted retroreflector in combination with other metrology systems to reduce engineering time for large CNC machine compensation.[8] As an extension of conventional laser trackers, Estler described absolute distance meters (ADMs), operating either in parallel with the interferometer or is used alone when interferometer resolution is not required.[9] The addition of ADMs to the interferometer provided the convenience of resetting the system without returning the retroreflector to the datum position.[6] Though considered to be the most reliable and well-established measurement systems, they are yet high cost and inefficient and bring huge challenges to the repair and maintenance of optical precision instruments. CCD cameras, with the measurement technique of photogrammetry, focus on the evaluation in two dimensions. Compared to the aforementioned systems, the vision system is more friendly to use, cost-efficient, and with a high accuracy.[10] Therefore, vision technology has been widely popularized in the field of industrial robotics research, especially for robot calibration.[11] However, machining in multi-stations makes real-time visual measurement and calibration unrealizable, and sources leading to a loss of absolute accuracy are usually concurrent (e.g., mechanical vibration, joint wear, tool displacement, etc.). Therefore, it has become very challenging on how to define the latest datum on workpiece using a vision system and compensate pose deviation rapidly and accurately when the robot updates its location.

The vision system of an industrial robot can be generally classified into two types of architecture: eye-to-hand and eye-in-hand. The eye-to-hand system requires a camera observing the robot within its workspace so it has a less precise but global sight of the scene, while the eye-in-hand system, with a camera rigidly mounted on the robot end-effector, has a partial but precise sight of the scene.[12] In contrast to the eye-to-hand system, the eye-in-hand system allows easier target recognition and inspection resulting from localization, resolution of occlusion problem, and limited depth-of-field, as well as spatial resolution in the large-volume robot motion workstation. However, multiple datum on the large-volume workpiece brings another challenge on how to make target markers mounted on the datum always being within the sight of camera.

In large-scale unstructured circumstances without intelligence, humans are indispensable since they are able to react intelligently to the unforeseen changes and accomplish skillful manipulation tasks.[13,14] Therefore, human–robot cooperation and interactions have shown rapid advances in robotic technologies. Most industrial human–robot interaction research focuses on the safety aspects in physical demonstrators,[15–17] while other researchers have focused directly on the safety system issue.[18–22] However, the increasing complexity of cooperative robotic systems requires systematic methods as well as supporting platform to experiment on and evaluate with. With simulation-based methods, robot models, including sensor and actuator models, are developed and then simulated on computers. Different experimental configurations can be easily applied to test and evaluate the system under development.[23] Mourtzis presented a development and testing of an augmented reality remote

https://doi.org/10.1017/S0263574719001371 Published online by Cambridge University Press

platform that can be used for providing systems maintenance service.[24] Busch et al. created a virtual simulation of industrial human–robot cooperation, presenting a welding cell where the human does the welding and the robot holds the objects that are to be united.[25] Ore et al. developed a new software demonstrator presenting a virtual simulation of industrial human–robot cooperation, and the results showed a decrease in operation time and increase in productivity.[26,27] It is worth mentioning that the existing commercial robot simulation software usually has its own data format and offers little possibilities in data exchange with other systems. To break through this barrier, a series of open-source 3D robot simulators are developed, such as V-Rep,[28,29] Gazebo,[30] Webots,[31] etc., offering much flexibility and customization to system development. Moreover, equipped with visualization interfaces, these software platforms have provided better interaction between human and robot, which means that human would operate a remote control through a visualized interface instead of working on site.

In this paper, a human-guided vision system is proposed to determine machining datum and compensate pose errors of the end-effector of robot, of which the feasibility and accuracy are validated in a sequence of simulations and experiments based on an eye-in-hand system. The system consists of three major parts: planar targets, a camera, and a handheld manipulator. The manipulator is a three-dimensional ergonomic mouse-like wireless displacement sensor that can be held in hand. Human can operate the end-effector of robot in 6-DOF using the manipulator so as to guide the camera to the place where it can catch sight of the planar target, which solves the problem of target loss in the camera field of view due to multi-datum on the large-volume workpiece. A virtual control platform called V-Rep, with an integrated development environment, is utilized to offer an intuitive and convertible environment for simulating and validating robotic tasks. The aforementioned 6-DOF handheld manipulator is integrated into the platform through an external API to facilitate the human–robot cooperation, which can be described as involving two steps: (i) through close-up images shown in the visible monitoring window, human can make appropriate manipulations on the end-effector until the target marker appears in sight; (ii) with image processing and error compensation algorithms, robot then compensates its pose deviation automatically and ultimately updates its location with respect to the datum. For traditional measurement systems based on cameras or LTS systems, it is necessary to put many cameras *in situ* in order to catch sight of the whole processing environment, especially in the circumstances of large-scale unstructured circumstances. However, the proposed method makes the system more flexible and can replace lots of cameras *in situ*. What's more, in circumstances where a target is lost in camera view, a traditional method cannot let the process continue, which will make the efficiency to drop. And compared with many cameras and expensive optical equipment, the method is more cost-effective.

The remainder of the paper is organized as follows. Section 2 describes the hybrid robot workstation together with the proposed human-guided vision system. Section 3 introduces the human–robot collaboration simulation in V-Rep. The vision-based pose estimation and compensation method is illustrated in Section 4. Simulations and experiments are shown in Section 5. The paper ends with concluding remarks.

2. System Description

Driven by the requirements of aeronautics, astronautics, and the shipping industry, aiming at manufacturing sophisticated and individualized large components, a novel 5-DOF hybrid robot, named TriMule, was designed in our previous work, which will be briefly introduced in this section. As a plug-and-play robotized module, TriMule was utilized in large-scale machining systems for local processing and can be fixed on a motion platform for multi-station machining.

2.1. TriMule

TriMule[4] is a novel 5-DOF hybrid robot that is composed of an over-constrained 1T2R (T, translation; R, rotation) parallel mechanism and a 2-DOF wrist, as shown in Fig. 1. The parallel mechanism comprises an actuated UPS limb and a stand-alone 1T1R planar linkage that contains two actuated RPR limbs and a properly constrained passive RP limb in-between. The base link of the 1T1R planar linkage is elaborately designed into a three-in-one part that locates the rear R joints of the two actuated RPR limbs, and the R and P joints of the RP limb, and at the same time it is connected by a

https://doi.org/10.1017/S0263574719001371 Published online by Cambridge University Press

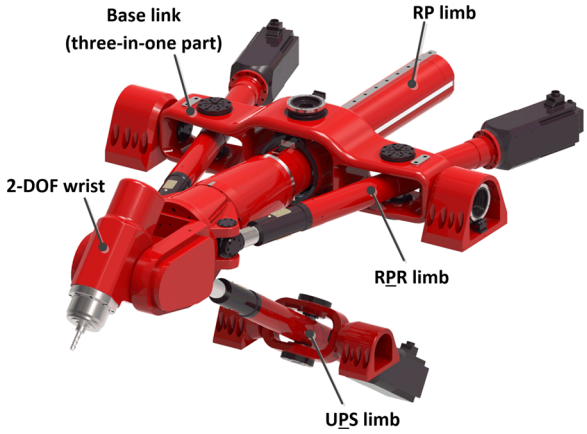

Fig. 1. 3D view of the TriMule robot. R, P, U, and S denote revolute, prismatic, universal, and spherical joints, respectively, and the underlined P denotes an actuated prismatic joint.

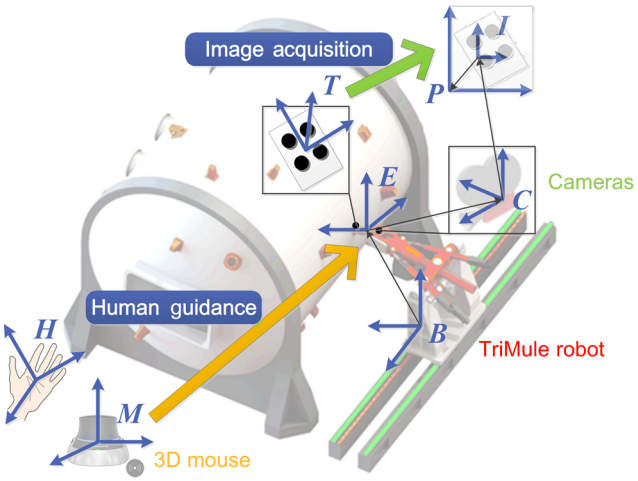

Fig. 2. Major components of the robot motion workstation and coordinate transformations among frames.

pair of R joints with the machine frame. R, P, and S stand, respectively, for revolute, prismatic, and spherical joints where the underlined joint represents the actuator.

2.2. *Proposed system*

The proposed system is composed of a TriMule robot, a long reference track, and a vision-based measurement system (see Fig. 2). The TriMule robot is mounted on a long reference track through casters and skids so that it can change its locations to perform multi-station machining. The vision-based measurement system is fixed on the end-effector of the robot, together with robot arms, composing the eye-in-hand system. So as to implement an intuitive way for human–robot interaction, a 3D mouse-like manipulator together with the visualization interface are integrated in the robot controller, with which human are capable of remotely controlling the end-effector of robot, guiding the cameras to "see" the target marker on workpiece, which is a significant premise for pose compensation of the end-effector of robot.

Among all the coordinate frames in the system, the 3D mouse frame M is fixed with respect to the world coordinate frame, while the TriMule robot base frame B is also fixed when it performs machining in a current processing station. Human manipulation on the 3D mouse is essentially the mapping from the hand frame H in M to the end-effector of robot frame E in B. The target marker frame T has been determined in advance with respect to the workpiece; together with transformation between the camera and the end-effector obtained by robot hand–eye calibration, the

https://doi.org/10.1017/S0263574719001371 Published online by Cambridge University Press

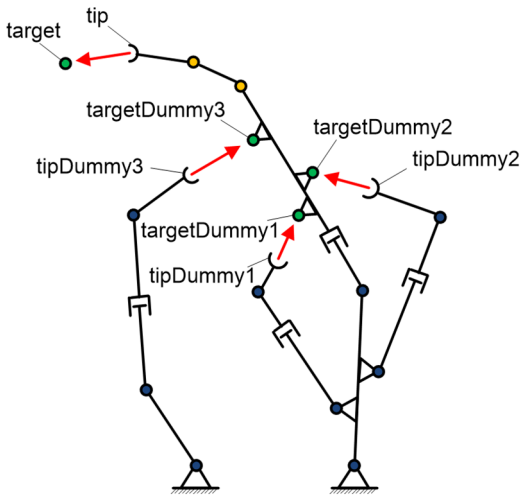

Fig. 3. A simplified mechanism diagram of TriMule, used for physical modeling in V-Rep. There are four kinematic chains in total, between which constraints are set through tip and target dummies. Constraints of the tip–target pairs are indicated by red arrows.

bridge between T and B that reflects the relative pose between the workpiece and the robot will be calculated.

3. Human–Robot Collaboration Simulation

3.1. Platform

The proposed system is a modular, including the robot module, robot platform module, external devices, and human. An open-source distributed platform framework can better adapt to system requirements. V-Rep is a virtual control platform, which has a distributed software framework and an open, integrated platform. Simulations are easy to implement on it, despite that module of the system has been changed. V-Rep provides an integrated development environment based on a distributed control architecture. The 5-DOF hybrid robot TriMule, as a user-defined model, is integrated in the V-Rep scene.

The TriMule CAD model (Fig. 1) was imported to V-Rep, and was rebuilt as a mechanism diagram as illustrated in Fig. 3. The rebuilding process includes segmentation, reorganization, and reconnection of model parts. There are four kinematic chains in topology, between which constraints are set through tip and target dummies, which are 3D coordinate frames fixed on chains. Constraints of the tip-target pairs are indicated by red arrows, showing their fully or partially overlapped relationships in position and orientation. A hierarchical tree showing connections among parts as well as the built 3D model in V-Rep are shown in Fig. 4.

Along with the distributed control architecture, the platform allows each model to be individually controlled via an embedded script, providing possibilities for synchronized, separate controls of multi-models in multiplex interaction robotized tasks. The software framework for the V-Rep is shown in Fig. 5, in which all the child scripts are initiated in the main script and then executed in the cascade mode.

3.2. 3D mouse integration

The mouse used for guidance of the vision system is an advanced wireless 6-DOF displacement sensor, named 3Dconnexion,[32] capable of detecting small inputs of human hand manipulation. The reference coordinate frame is shown in Fig. 6, where axis 0, 1, 2 are translation axes and 3, 4, 5 are rotation axes. The integrated architecture of the hardware and software is illustrated in Fig. 7, with the left side showing the communication between 3Dconnexion mouse and robot controller (i.e., V-Rep) based on a wireless receiver, and the right side illustrating the framework of the Lua-SDL2 libraries together with other necessities required by controlling the script in V-Rep.

The core of the software architecture is Lua-SDL2, a Lua extension library of SDL[33] containing a class for joystick, which implements initialization, identification of the 3Dconnexion mouse, and

https://doi.org/10.1017/S0263574719001371 Published online by Cambridge University Press

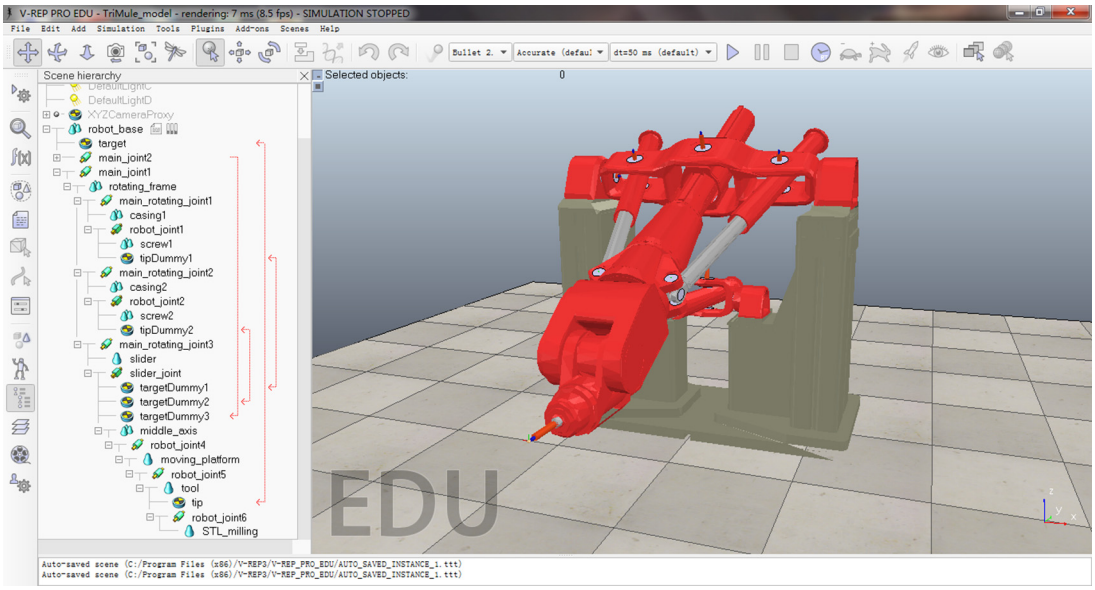

Fig. 4. 3D visualization of a graphical interface in V-Rep. The right side shows the physical model of a TriMule robot, while the left side shows the hierarchical tree containing robot components (i.e., base, links and joints).

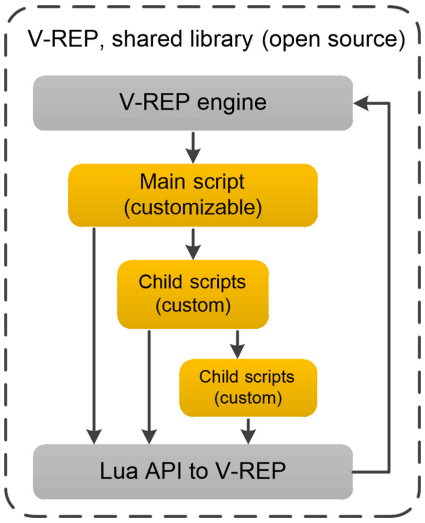

Fig. 5. Software controller framework of the V-Rep simulator, where all the child scripts are initiated in the main script and executed in cascade mode.

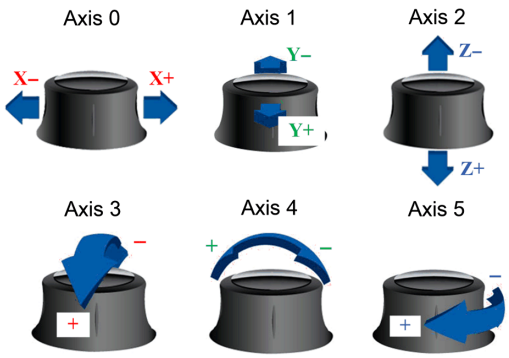

Fig. 6. Reference coordinate frame of a 3Dconnexion mouse, where axis 0, 1, 2 represent the translation axes and 3, 4, 5 represent the rotation axes.

https://doi.org/10.1017/S0263574719001371 Published online by Cambridge University Press

Table I. Correspondence between the six axes of 3Dconnexion mouse and 5 DOF of TriMule relative to the robot base coordinate frame, whose three axes are represented by X_B, Y_B, Z_B.

Axis index of 3Dconnexion mouse	**Degree of freedom of TriMule robot**
Axis 0	Translation along Y_B
Axis 1	Translation along X_B
Axis 2	Translation along $-Z_B$
Axis 3	Rotation around Y_B
Axis 4	Rotation around X_B
Axis 5	Null

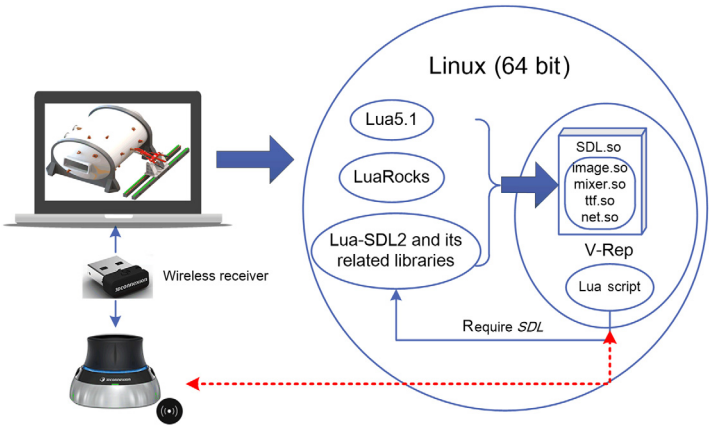

Fig. 7. An integrated architecture of the 3Dconnexion mouse both in hardware and software.

returns corresponding signal values depending on multiple types of trigger events, for example, multi-axis movement, button press events, etc.

The correspondence between the six axes of the mouse and 5 DOF of TriMule robot is shown in Table I. Duo to an ergonomic design of the 3Dconnexion mouse, translations and rotations of the end-effector are accomplished in human perspective, and the visualized 3D scene in V-Rep offers a possibility of real-time monitoring of robot status so that operation feedback can be made by human.

4. Vision-Based Measurement System

Due to the movement of robot platform among multi-stations, the camera mounted on the robot end-effector may lose sight of the target datum. To solve this problem, guidance information is provided to the robot at the first step, leading the end-effector of robot to an approximate pose round the target datum. And for the second step, the vision-based measurement system takes on a fine adjustment of the robot for a precise and robust measurement of target datum and error compensation.

Vision-based measurement and calibration are essential processes for assuring accuracy in robot machining, especially when they are applied in multi-station machining because uncertain factors (e.g., mechanical vibration, joint wear, tool displacement, etc.) may lead to errors in both position and orientation of the end-effector.

4.1. Robot hand–eye calibration

When the camera undergoes a motion $A = [\boldsymbol{R}_C, \boldsymbol{t}_C]$, which can be estimated, the end-effector of robot undergoes a motion $B = [\mathbf{R}_E, \mathbf{t}_E]$ that can be obtained from the robot controller, where $\boldsymbol{R}$ is a 3×3 rotation matrix and $\boldsymbol{t}$ is a 3×1 translation matrix. With hand–eye transformation $\boldsymbol{X} = [\boldsymbol{R}_x, \boldsymbol{t}_x]$, there is a homogenous matrix equation:

$$\boldsymbol{AX} = \boldsymbol{XB} \tag{1}$$

where $\boldsymbol{X}$ is to be solved, representing the transformation from camera to the end-effector frame.

https://doi.org/10.1017/S0263574719001371 Published online by Cambridge University Press

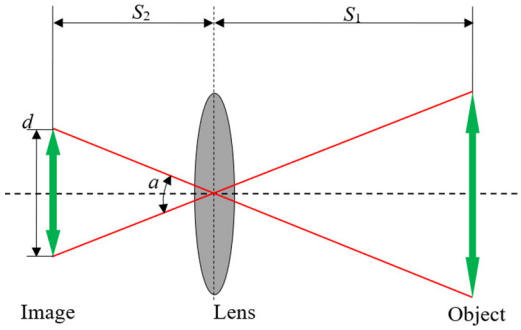

Fig. 8. A pinhole model of the perspective camera.

When applied to motion i, the above equation turns into:

$$\begin{cases} \boldsymbol{R}_{Ci}\boldsymbol{R}_x = \boldsymbol{R}_x\boldsymbol{R}_{Ei} \\ \boldsymbol{R}_{Ci}\boldsymbol{R}_x + \boldsymbol{t}_{Ci} = \boldsymbol{R}_x\boldsymbol{R}_{Ei} + \boldsymbol{t}_x \end{cases}. \tag{2}$$

To solve the equation, Tsai–Lenz[34] method has been proposed and popularized; $\boldsymbol{R}_x$ and $\boldsymbol{t}_x$ are successively calculated using least-squares techniques in two-stage solution.

4.2. Pose estimation

The imaging process can be simplified as a pinhole model (see Fig. 8). S_1 and S_2 are, respectively, the distance from linear lens to target object and image plane; d is the size of image; F is the focal length of lens. When a lens is focusing, $S_2 = F$. Due to geometrical relations, the angle of view α can be expressed as:

$$\alpha = 2\arctan\left(\frac{d/2}{F}\right). \tag{3}$$

For any point j on the target, coordinates on the pixel plane are expressed as (u_j, v_j), which is obtained from images. With resolution $(r_{xj}, r_{yj})$of the pixel plane in both X- and Y-axis known, the corresponding angular position (β_{xj}, β_{yj}) on the pixel plane can be calculated:

$$\begin{cases} \beta_{xj} = \arctan\left[\left(\frac{2u_j}{r_{xj}} - 1\right) \cdot \tan\frac{\alpha}{2}\right] \\ \beta_{yj} = \arctan\left[\left(\frac{2v_j}{r_{yj}} - 1\right) \cdot \tan\frac{\alpha}{2}\right] \end{cases}. \tag{4}$$

With the obtained depth information $\varepsilon \in [\mathbf{0}, \mathbf{1}]$ of the camera and the preset near-distance Z_{near} and far-distance Z_{far}, the 3D coordinates with respect to the camera coordinate frame $^{(X_C,Y_C,Z_C)}$ are derived:

$$\begin{cases} Z_C = (Z_{far} - Z_{near})\boldsymbol{\varepsilon} \\ X_C = Z_C\mathbf{tan}(\beta_x) \\ Y_C = Z_C\mathbf{tan}(\beta_y) \end{cases}. \tag{5}$$

The 3D coordinates are then homogenized and converted to coordinates (X_B, Y_B, Z_B) in the robot base frame:

$$\begin{bmatrix} X_B \\ Y_B \\ Z_B \\ 1 \end{bmatrix} = {}^B_E\boldsymbol{A}\boldsymbol{X}^{-1}\begin{bmatrix} X_C \\ Y_C \\ Z_C \\ 1 \end{bmatrix} \tag{6}$$

where ${}^B_E\boldsymbol{A} \in \boldsymbol{R}^{4\times4}$ is the transformation matrix from base to the end-effector frame, acquired straightforward from the robot controller. With the cross-product of two vectors $\boldsymbol{\tau}_1 \in \boldsymbol{R}^{3\times1}$ and $\boldsymbol{\tau}_2 \in \boldsymbol{R}^{3\times1}$

https://doi.org/10.1017/S0263574719001371 Published online by Cambridge University Press

not collinear on the plane, the normal vector $\boldsymbol{n} \in \boldsymbol{R}^{3\times 1}$ that is perpendicular to the target marker plane can be expressed as:

$$\boldsymbol{n} = \boldsymbol{\tau}_1 \times \boldsymbol{\tau}_2, \tag{7}$$

which contains orientation information of the target marker.

4.3. Pose error compensation

Robot machining programs are written with respect to a workpiece system which are then executed by a robot controller, where control is made in Cartesian or joint workspace. However, the robot workspace may sustain deviation due to mechanical vibration, joint wear, or tool displacement, etc., which might be aggravated in multi-station circumstances. It is worth noting that rather than presenting an error on a certain location (i.e., datum), the deviation may result in pose errors of end-effector of the robot on the entire machining trajectory. As regards the robotic drilling process, the pose error on datum may cause error on each hole, resulting in a high rate of discarded large-scale workpiece. Therefore, pose error compensation aims at reducing pose errors on the entire processing trajectory with the estimated pose on datum.

In a traditional robot machining process without compensation, the robot controller firstly controls its end-effector to reach the initial pose (i.e., machining datum). The end-effector frame at this pose is expressed as $\Re$ and for each point k on the trajectory, a homogenous matrix $\boldsymbol{\xi}_{\Re k} \in \boldsymbol{R}^{4\times 4}$ represents the position and orientation at this point with respect to $\Re$. With pose estimation on the machining datum, the end-effector frame transforms to $\Re'$ and, correspondingly, the position and orientation with respect to the new frame turns to $\boldsymbol{\xi}_{\Re' k} \in \boldsymbol{R}^{4\times 4}$. A compensation matrix $\boldsymbol{M} \in \boldsymbol{R}^{4\times 4}$ is proposed to define the homogenous transformation from $\Re$ to $\Re'$, which yields the transformation equation:

$$\boldsymbol{\xi}_{\Re k} = \boldsymbol{M} \cdot \boldsymbol{\xi}_{\Re' k} \tag{8}$$

where $\boldsymbol{M}$ can be calculated with the theoretical and estimated poses of three points on target marker. $\boldsymbol{\xi}_{\Re' k}$ represents a pose at each point on the theoretical machining trajectory, which is regarded as known, and the compensated pose $\boldsymbol{\xi}_{\Re k}$ can be deducted to update the robot machining trajectory.

5. Implementation

5.1. Workflow

Implements described in this paper are operated on V-Rep since it offers an intuitive and convertible environment for simulating and validating robotized tasks. Figure 9 shows the workflow on a V-Rep experiment platform. As shown, the major three modules are included in the main program: (I) vision-based human guidance, (II) image processing, (III) pose estimation and error compensation. Among them, (I) and (III) have already been described, while image processing is accomplished by applying a built-in filter in V-Rep. A virtual vision sensor normally produces two images at each simulation pass: a color image and a depth map. It is a flexible way to retrieve the images and associate them with a filter, which can be composed by combining several components. A simple filter can be illustrated in three components: (i) transfer input image to work image; (ii) invert work image; (iii) transfer work image to output image. For the target marker with circle features used in this paper, edge detection together with blob detection[35] components are added on the work image, and specific values (i.e., positions of the center of circle) are accessed through API calls.

Control algorithms of the 5-DOF hybrid robot model are written in Lua scripts and run on a CPU with a frequency of 50 Hz. Besides the abovementioned modules, other embedded functions and libraries, such as inverse kinematics, open motion planning library (OMPL), user interfaces (UI), etc., are also called to facilitate the whole human–robot collaboration simulation.

5.2. Experiments

5.2.1. Experimental design. In this section, experiments are carried out to assess the feasibility of human-robot collaboration, pose compensation performance, and pose estimation accuracy of the end-effector of TriMule. The 3Dconnexion mouse is connected to the simulator through a wireless receiver so that remote controlling is allowed. The angle of view of the virtual camera is set to 60°,

https://doi.org/10.1017/S0263574719001371 Published online by Cambridge University Press

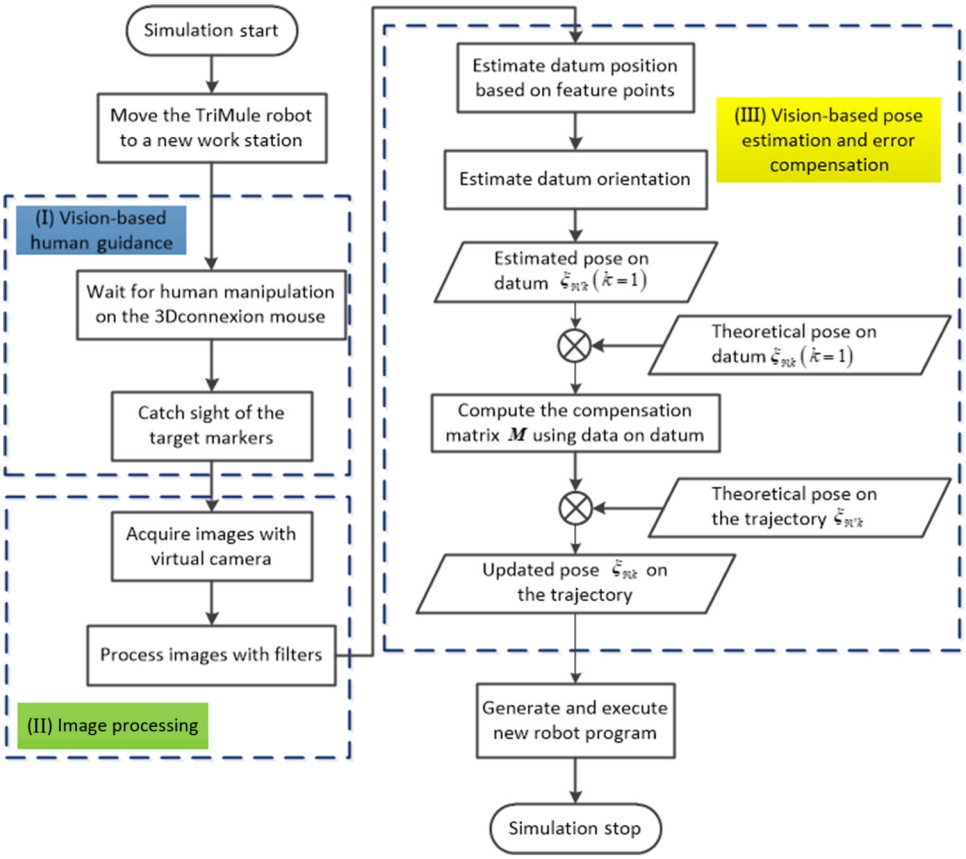

Fig. 9. A general workflow of the entire experiment based on the proposed method in V-Rep.

positions of near and far plane to 0.2 and 0.6 m respectively, and resolutions in X and Y direction to both 512.

The experiment is designed for drilling application. To simplify the implementation and focus mainly on pose estimation and compensation algorithms, the robot module is located at one station and is ordered to drill four holes on a flat steel plate. Three assumptions on the deviation of robot frame are set beforehand, respectively 2 mm along X-, Y- and Z-axes, 0.3° on both β and γ, 5 mm along X-, Y- and Z-axes, 0.3° on both β and γ, and 5 mm along X-, Y- and Z-axes, 0.5° on both β and γ, where β and γ represent pitch and yaw of the Euler angle, resulting in pose errors in the end-effector frame. These deviations of robot trajectory have been preset in the controller. To obtain precision of the end-effector before and after pose estimation and compensation, errors at four drilling holes are calculated respectively. As Eq. (9) shows, e represents an error before compensation on n points on the target, while e' represents an error after compensation, and X_{i0} is the theoretical position of target points, X_i and $X_i^{'}$ are vision-detected positions, respectively. Also, the performance of the entire processing trajectories is also compared and evaluated.

$$e = \frac{\sum_{i=1}^{n}(X_i - X_{i0})}{n} \quad e' = \frac{\sum_{i=1}^{n}(X_i' - X_{i0})}{n} \quad n = 4 \,. \tag{9}$$

Moreover, in order to ensure accuracy of pose estimation, an experiment is carried out in which the end-effector of TriMule is manipulated to 10 different locations using the 3Dconnexion mouse, and errors between theoretical and estimated poses are calculated as described in Section 4.2.

5.2.2. Analysis of results. It is clear that the motion of a robot workstation has a significant effect on the field of view of the camera, especially for the eye-in-hand system, for which vision-based human guides are necessary. In the experiment, the output images are retrieved in the 3D visualized environment in 50 Hz, based on which human can operate feedback upon the environment by manipulating the 3Dconnexion mouse in 6-DOF. Figure 10 shows the rendering graphic view of the camera

https://doi.org/10.1017/S0263574719001371 Published online by Cambridge University Press

Table II. Position errors at four drilling holes and orientation error on the flat steel plate before and after compensation when deviation of robot frame set to 2 mm along X-, Y- and Z-axes, 0.3° on both β and γ of Euler angle.

	Without compensation				**With compensation**			
	Position error [mm]				**Position error [mm]**			
No.	***X***	***Y***	***Z***	**Orientation error [°]**	***X***	***Y***	***Z***	**Orientation error [°]**
1	1.9	1.7	5.5	0.02071	1.4	0.4	3.1	0.01750
2	2.8	2.8	5.8		0.8	0.1	1.9	
3	1.8	1.7	5.9		0.7	0.2	0.7	
4	2.8	2.7	5.8		0.3	0.7	1.1	

Table III. Position errors at four drilling holes and orientation error on the flat steel plate before and after compensation when deviation of robot frame set to 5 mm along X-, Y- and Z-axes, 0.3° on both β and γ of Euler angle.

	Without compensation				**With compensation**			
	Position error [mm]				**Position error [mm]**			
No.	***X***	***Y***	***Z***	**Orientation error [°]**	***X***	***Y***	***Z***	**Orientation error [°]**
1	2.9	4.8	2.5	0.02071	0.6	0.0	2.3	0.01735
2	5.8	5.8	2.8		0.5	0.5	0.4	
3	4.8	4.7	2.9		0.8	0.0	1.3	
4	5.8	5.7	3.2		0.8	0.5	0.4	

Table IV. Position errors at four drilling holes and orientation error on the flat steel plate before and after compensation when deviation of robot frame set to 5 mm along X-, Y- and Z-axes, 0.5° on both β and γ of Euler angle.

	Without compensation				**With compensation**			
	Position error [mm]				**Position error [mm]**			
No.	***X***	***Y***	***Z***	**Orientation error [°]**	***X***	***Y***	***Z***	**Orientation error [°]**
1	2.8	4.7	7.4	0.03616	0.8	0.2	2.9	0.01759
2	6.4	6.4	8.0		1.6	0.0	1.5	
3	4.7	4.5	8.0		0.4	0.1	1.2	
4	6.3	6.2	8.6		0.3	0.6	0.3	

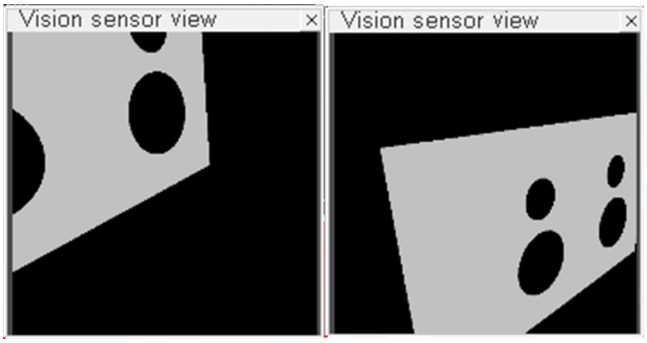

Fig. 10. Rendering 3D graphics in V-Rep. The left picture shows the view before human guidance, where the target is not totally caught sight of, while the right picture shows the view after human guiding the camera.

https://doi.org/10.1017/S0263574719001371 Published online by Cambridge University Press

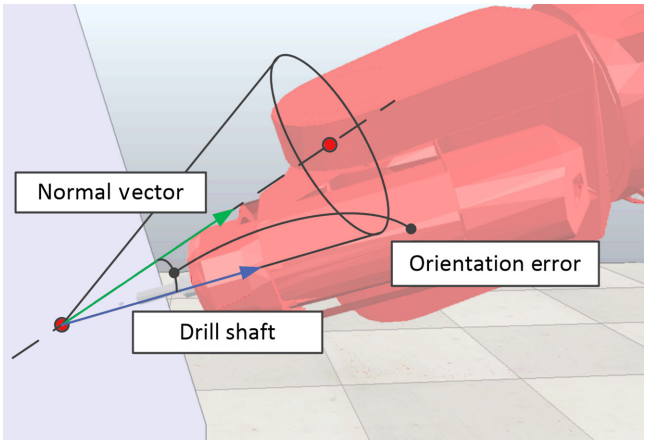

Fig. 11. Orientation error expressed as an angular deviation between normal vector of the processing steel plate and the drilling shaft.

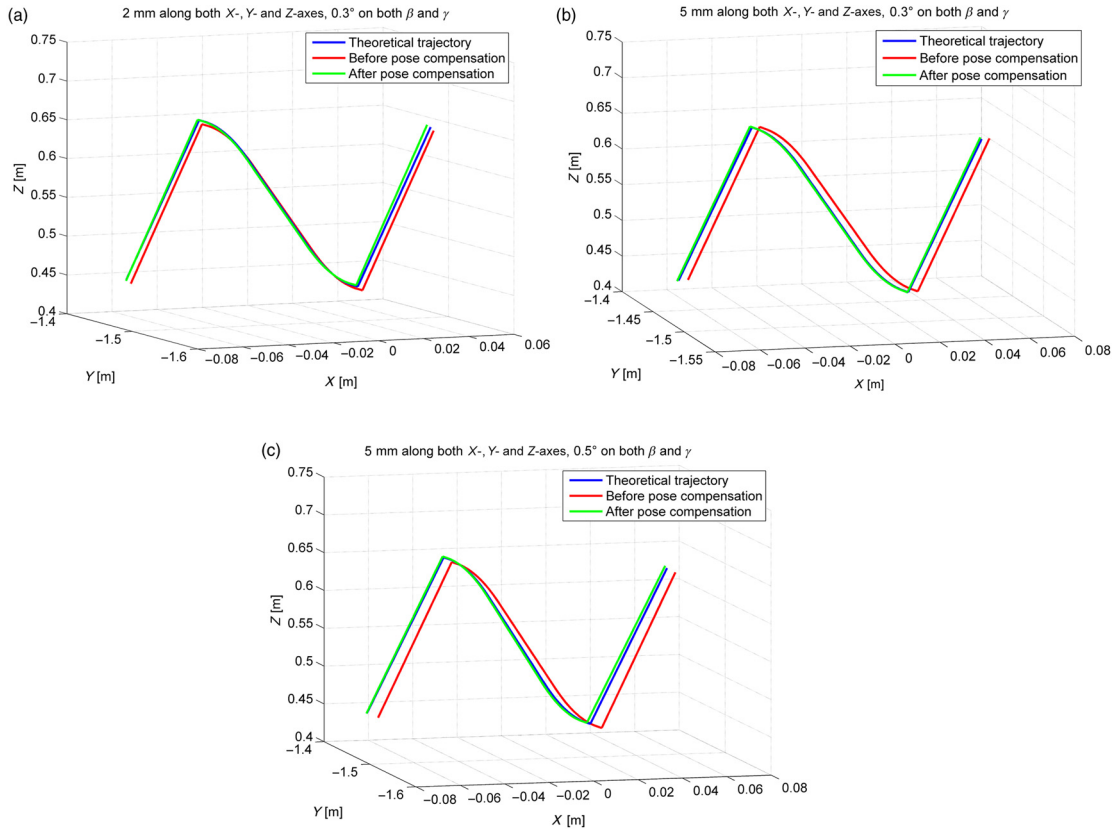

Fig. 12. Robot drilling trajectories with the three assumptions of the deviation of robot frame: (a) 2 mm along X-, Y- and Z-axes, 0.3° on both β and γ; (b) 5 mm along X-, Y- and Z-axes, 0.3° on both β and γ; (c) 5 mm along X-, Y- and Z-axes, 0.5° on both β and γ.

in V-Rep before and after human guidance. With detecting inputs as small as 4 microns and rapid signal transmission combined with 2.4 GHz wireless technology, the 3Dconnexion mouse is capable of mapping sensor displacements to the robot space with a high robust and real-time performance.

Tables II–IV record, respectively, position errors at four drilling holes and orientation error on the flat steel plate before and after compensation under three different preset biases in the robot frame, as mentioned in Section 5.2.1. The position error is calculated and expressed in X-, Y- and Z-axes. Moreover, as an important part of error estimation in the drilling process, orientation error is

https://doi.org/10.1017/S0263574719001371 Published online by Cambridge University Press

Table V. Mean position errors at four points and orientation errors of the target marker in 10 sets of experiment.

	Position error [mm]			
No.	***X***	***Y***	***Z***	**Orientation error [°]**
1	0.797	0.172	0.985	0.01698
2	0.566	0.191	1.110	0.01411
3	0.937	0.166	1.032	0.02150
4	1.094	0.167	0.800	0.02628
5	0.933	0.036	1.433	0.01307
6	0.551	0.289	2.431	0.00606
7	0.447	0.127	2.028	0.02072
8	0.597	0.218	2.412	0.00958
9	0.814	0.175	2.379	0.01422
10	0.915	0.245	2.213	0.01063
Mean	0.7651	0.1786	1.6823	0.01532

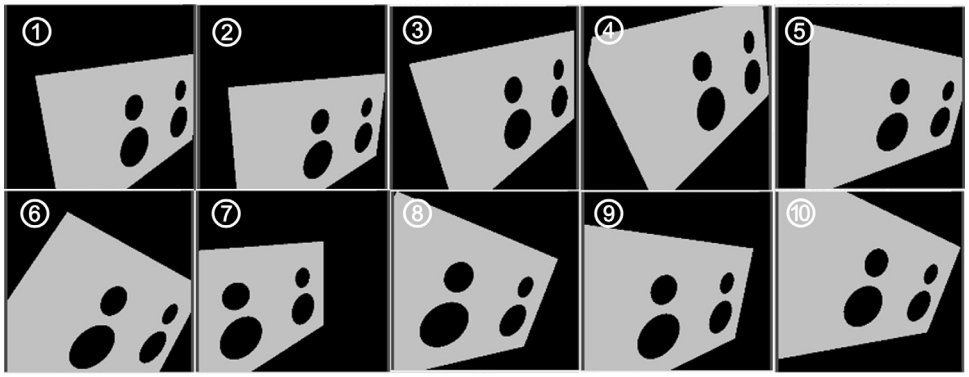

Fig. 13. Ten images acquired by the virtual camera from 10 perspectives.

expressed as an angular deviation between normal vector of the steel plate and the drilling shaft (see Fig. 11), which is within the conical space with normal vector at the drilling point as rotation axis.

It can be seen that under different assumptions of robot frame deviation, the position error of end-effector before compensation can be very large, reaching almost 8.6 mm in one direction, and orientation error 0.03616°. With no attempt being made to align the robot motion platform, the preset deviation of robot frame is random and leads to an uncertain end-effector pose error. However, with the proposed pose estimation and compensation method, the error greatly reduces to 0.3 mm in one direction and 0.01759° in angle and is basically maintained around this value despite different deviations of the robot frame.

Due to an inaccuracy in reference tracking and actual motion error, the robot platform may have deviations along the straight line and height direction of the reference track, as well as rotation deviations around the reference track and around the perpendicular direction of the reference track. If there is no pose estimation and error compensation, the machining trajectory will be offset to a great extent, resulting in large deviations directly. The reduction of pose error is shown more clearly on the entire processing trajectories in Fig. 12, where (a), (b), (c), respectively, correspond with the abovementioned three sets of experiments. It is visible that without pose estimation and compensation, the trajectory suffers a large deviation in the 3D workspace, while the generated trajectory after compensation coincides with the theoretical one to a great extent.

Notably, though the proposed vision-based compensation method can reduce the end-effector pose error under a large deviation of the robot platform caused by mechanical vibration, joint wear, tool displacement, etc., there still exists a principle error that sources from pose estimation. So as to estimate the error, a sample containing 10 images are captured (see Fig. 13) by simply detecting the

https://doi.org/10.1017/S0263574719001371 Published online by Cambridge University Press

target marker using robot vision. The mean position errors at four points and orientation errors of the target marker are calculated (Table V).

Means of errors are calculated using the acquired data from 10 sets of experiments, reflecting the magnitude of pose estimation error, whose position error is below 1.6823 mm in one direction and orientation error is 0.01532° in angle. It is worth noting that this error is at a specific point. Since the generation of an updated trajectory depends on the measured pose on the datum point, pose errors on other points of the trajectory will be amplified in some degree, which means the global errors might be much higher than the one on datum. The successively increasing trend on errors at the four drilling holes shown in Tables II– IV and Fig. 12 is consistent with the analysis.

In addition, errors introduced by the 3D mouse were not considered, because the function of the mouse is to guide the end-effector of robot to an approximate pose round the target datum which would not have a great effect on the ultimate precision as long as the visual measurement is carried on as expected.

6. Conclusions

To improve ultimate accuracy, a human-guided, high-precision vision system is integrated to the TriMule robot to measure machining datum and compensate pose errors of the TriMule end-effector. The system contains mainly a camera mounted at the end-effector that can be manipulated by human with a 6-DOF 3Dconnexion mouse. Human guidance was tested on the V-Rep environment to validate the feasibility of human–robot collaboration, which showed a robust and real-time performance on mapping human manipulation to the end-effector of robot. In multi-station robot machining, due to the fact that uncertain factors (e.g., mechanical vibration, joint wear, tool displacement, etc.) may lead to errors of the robot end-effector in both position and orientation, pose estimation and compensation methods are proposed and experiments are implemented under the assumption of a preset deviation of the robot platform. Results showed a great reduction in the pose error compared to the one without pose estimation and compensation. With the deviation of robot frame set to 5 mm along X-, Y- and Z-axes, 0.5° on both β and γ of Euler angle, the position error decreased from 8.6 to 0.3 mm along Z-axis, and orientation error decreased from 0.03616° to 0.01759°. A comparison of results for the three groups of experiments also indicated that the proposed vision-based pose estimation and error compensation method provided immunity to mobility deviations of robot workstation for large-scale industrial applications. The principle error caused by pose estimation was also obtained, with position error below 1.6823 mm in one direction and orientation error 0.01532° in angle. The principle error was mainly caused by image processing and target detection, which is an algorithm-level issue to be taken into account. In the future, more work should concentrate on decreasing the principle error, which is also a factor affecting machining accuracy.

Acknowledgements

This work was supported by the National Key Research and Development Program (2017YFE0111300), National Natural Science Foundation of China (51775376 and 51420105007), and EU H2020 project (734272).

References

1. M. Summers, "Robot Capability Test and Development of Industrial Robot Positioning System for the Aerospace Industry," *SAE Aerospace Manufacturing and Automated Fastening Conference*, Texas, USA, Paper No. 01-3336 (2005).
2. K. E. Neumann, "The Key to Aerospace Automation," *SAE Aerospace Manufacturing and Automated Fastening Conference and Exhibition*, Detroit, USA, Paper No. 01-3144 (2006).
3. K. E. Neumann, "Tricept Application," *Proceedings of the 3rd Chemnitz Parallel Kinematics Seminar*, Zwickau, Germany (2002) pp. 547–551.
4. T. Huang, C. Dong, H. Liu, X. Qin, J. Mei, Q. Liu and M. Wang, "Five-degree-of-freedom hybrid robot with rotational supports," United States Patent, No.: US 9,943,967 B2 (2018).
5. A. Frommknecht, J. Kuehnle, I. Effenberger and P. Sergej, "Multi-sensor measurement system for robotic drilling," *Rob. Comput.-Integr. Manuf.* **47**, 4–10 (2017).
6. M. Galetto, "Advances in large-scale metrology – Review and future trends," *CIRP Ann. Manuf. Technol.* **65**(2), 643–665 (2016).
7. M. Vincze, J. P. Prenninger and H. Gander, "A laser tracking system to measure position and orientation of robot end effectors under motion," *Int. J. Rob. Res.* **13**(4), 305–314 (1994).

https://doi.org/10.1017/S0263574719001371 Published online by Cambridge University Press

8. R. Flynn, "Synthesizing metrology technologies to reduce engineering time for large CNC machine compensation," *SAE Int. J. Mater. Manuf.* **5**(1), 49–59 (2011).
9. W. T. Estler, K. L. Edmundson, G. N. Peggs and D. H. Parker, "Large-scale metrology – An update," *CIRP Ann. Manuf. Technol.* **51**(2), 587–609 (2002).
10. X. Zhang, Y. Song, Y. Yang and H. Pan, "Stereo vision based autonomous robot calibration," *Rob. Auton. Syst.* **93**, 43–51 (2017).
11. Z. S. Roth, H. Zhuang and K. Wang, "Simultaneous calibration of a robot and a hand-mounted camera," *T-RA* **11**(5), 649–660 (1995).
12. G. Flandin, F. Chaumette and E. Marchand, "Eye-in-Hand/Eye-to-Hand Cooperation for Visual Servoing," *Proceedings of the IEEE International Conference on Robotics and Automation*, San Francisco, CA, USA (2000) pp. 2741–2746.
13. X. Li and C. C. Cheah, "Human-Guided Robotic Manipulation: Theory and Experiments," *Proceedings of the IEEE International Conference on Robotics and Automation*, Hong Kong, China (2014) pp. 4594–4599.
14. X. Li, G. Chi, S. Vidas and C. C. Cheah, "Human-guided robotic comanipulation: Two illustrative scenarios," *IEEE Trans. Control Syst. Technol.* **24**(5), 1751–1763 (2016).
15. J. Krüger, T. K. Lien and A. Verl, "Cooperation of human and machines in assembly lines," *CIRP Ann. Manuf. Technol.* **58**(2), 628–646 (2009).
16. M. Morioka and S. Sakakibara, "A new cell production assembly system with human-robot cooperation," *CIRP Ann. Manuf. Technol.* **59**(1), 9–12 (2010).
17. C. Zwicker and G. Reinhart, "Human-Robot-Collaboration System for a Universal Packaging Cell for Heavy Electronic Consumer Goods," **In**: *Enabling Manufacturing Competitiveness and Economic Sustainability* (Springer, Cham, Switzerland, 2014).
18. M. Fischer and D. Henrich, "3D Collision Detection for Industrial Robots and Unknown Obstacles Using Multiple Depth Images," **In:** *Advances in Robotics Research* (Springer, Berlin, Heidelberg, 2009).
19. N. Pedrocchi, F. Vicentini, M. Malosio and L. M. Tosatti, "Safe human-robot cooperation in an industrial environment," *Int. J. Adv. Rob. Syst.* **10**(1972), 1–13 (2013).
20. B. Schmidt and L. Wang, "Active Collision Avoidance for Human-Robot Collaborative Manufacturing," *Proceedings of the 5th International Swedish Production Symposium*, Linköping, Sweden (2012) pp. 81–86.
21. T. Salmi, O. Väätäinen, T. Malm, J. Montonen and I. Marstio, "Meeting New Challenges and Possibilities with Modern Robot Safety Technologies," **In**: *Enabling Manufacturing Competitiveness and Economic Sustainability* (Springer, Cham, Switzerland, 2014).
22. X. Hu and B. P. Zeigler, "A simulation-based virtual environment to study cooperative robotic systems," *Integr. Comput. Aided Eng.* **12**(4), 353–367 (2005).
23. D. Mourtzis, N. Papakostas, D. Mavrikios, S. Makris and K. Alexopoulos, "The role of simulation in digital manufacturing: Applications and outlook," *Int. J. Comput. Integr. Manuf.* **28**(1), 3–24 (2015).
24. D. Mourtzis, V. Zogopoulos and E. Vlachou, "Augmented reality application to support remote maintenance as a service in the robotics industry," *Procedia CIRP*. **63**, 46–51 (2017).
25. F. Busch, S. Wischniewski and J. Deuse, "Application of a Character Animation SDK to Design Ergonomic Human-Robot-Collaboration," *Proceedings of the 2nd International Digital Human Modeling Symposium*, Ann Arbor, MI (2013) pp. 1–7.
26. F. Ore, L. Hanson, N. Delfs and M. Wiktorsson, "Virtual Evaluation and Optimisation of Industrial Human-Robot Cooperation: An Automotive Case Study," *Proceedings of the 2nd International Digital Human Modeling Symposium*, Tokyo, Japan (2014) pp. 1–8.
27. F. Ore, L. Hanson, N. Delfs and M. Wiktorsson, "Human industrial robot collaboration – Development and application of simulation software," *Int. J. Hum. Factors Modell. Simul.* **5**(2), 164–185 (2015).
28. M. Freese, S. Singh, F. Ozaki and N. Matsuhira, "Virtual Robot Experimentation Platform V-REP: A Versatile 3D Robot Simulator," *Proceedings of the International Conference on Simulation, Modeling, and Programming for Autonomous Robots*, Darmstadt, Germany (2010) pp. 51–62.
29. E. Rohmer, S. P. N. Singh and M. Freese, "V-REP: A Versatile and Scalable Robot Simulation Framework," *Proceedings of the IEEE/RSJ International Conference on Intelligent Robots and Systems (IROS)*, Tokyo, Japan (2013) pp. 1321–1326.
30. N. Koenig and A. Howard, "Design and Use Paradigms for Gazebo, an Open-Source Multi-Robot Simulator," *Proceedings of the IEEE/RJS International Conference on Intelligent Robots and Systems (IROS)*, Sendai, Japan (2004) pp. 2149–2154.
31. O. Michel, "Cyberbotics ltd. webots^{TM}: Professional mobile robot simulation," *Int. J. Adv. Rob. Syst.* **1**(1), 39–42 (2004).
32. 3Dconnextion, "3Dconnexion: The World's First Wireless 3D Mouse," http://www.3dconnexion.com/products/spacemouse/spacemousewireless.html. accessed 14 June 2018.
33. Simple DirectMedia Layer, "About SDL," https://wiki.libsdl.org/FrontPage, accessed 14 June 2018.
34. R. Tsai and R. Lenz, "A new technique for fully autonomous and efficient 3D robotics hand/eye calibration," *IEEE Trans. Rob. Autom.* **5**(3), 345–358 (1989).
35. R. Grycuk, M. Gabryel, M. Korytkowski, R. Scherer and S. Voloshynovskiy, "From Single Image to List of Objects Based on Edge and Blob Detection," *International Conference on Artificial Intelligence and Soft Computing*, Zakopane, Poland (2014) pp. 605–615.

https://doi.org/10.1017/S0263574719001371 Published online by Cambridge University Press